

Study of the electronic and optical properties of half-Heusler alloys CoCrSn.

Ahmed Elhag^{1*}, Abdullah Rafia B Al-mutairi¹

Department of physics, college of science. Qassim University, Buridah 51452, Saudi Arabia

*Corresponding author, E- mail: af.elhag@qu.edu.sa

Abstract

We investigate the electronic, structure and optical properties of half-Heusler compound CoCrSn using the Full-Potential Linearized Augmented Plane Wave Method (FLAPW) within generalized gradient approximation (GGA) and generalized gradient approximation including Hubbard U-parameter (GGA + U) for the exchange correlation term of the effective Hamiltonian based on the density functional theory (DFT). Structural optimizations were carried out for both compound which revealed that the ferromagnetic (FM) state was more stable than nonmagnetic (NM) state. So, in the (FM) state the equilibrium lattice parameter was 5.8540 Å for CoCrSn. The alloy was found to be nearly half metallic (HM) at equilibrium cell volume. Basic optical properties like dielectric function, reflectivity, energy loss function, absorption coefficient were hence determined for a range of photon energy up to 12 eV (ultraviolet region).

Keywords: Optical, alloys, electronic, CoCrSn, half-Heusler

1. Introduction

During the last three decades, the half-Heusler (HH) alloys have drawn a growing attention of researcher in the field of spintronics (spin electronics) duo to their high Curie temperature and high compatibility with the lattice of two element semiconductor, which is a privilege for the two epitaxial growth of (HM) thin films on semiconductor substrates spin electronics devices. [1, 2]. Based on the electronic properties calculations, many half-Heusler alloys, such as NiCrTe, [3, 4] FeCrSe [5] and CoMnSb, [6] were predicted to be HM materials. It is well known that, stable half metallicity is an essential property required in the construction of spintronic devices. Therefore, it is necessary to study the stability in searching for new HM materials valid for spintronics application. Extensive research effort was put on investigating the HM character of HH alloys. Zhang et. al. found that NiCrP, NiCrTe and NiCrSe are HM ferrimagnets and that, the half-metallicity of NiCrP and NiCrTe can be kept as long as the change of lattice

constant is not more than 2–3%. [5] Huang et al. found the half metallicity of FeCrSe is stability when lattice constant is changed about -4.56 to 3.52% , and the larger tetragonal distortion does not destroy the HM properties. [5]. Recently, some CoCr-based half-Heusler alloys have also been theoretically predicted to be half-metals. Yao and colleagues found CoCrP and CoCrAs are HM at the range of lattice constants from 5.16 \AA to 5.78 \AA and 5.13 \AA to 5.81 \AA , respectively.[6] Feng et al. proved the half-metallicity of CoCrSi and CoCrGe and found that CoCrGe can maintain its half-metallicity when its lattice constants are changed by -3.1 to 4.7% relative to the equilibrium lattice constant.[7] However, these investigations on HM stability of CoCr-based half-Heusler alloys are mainly focused on HM gap, neglecting the mechanical stability of the HM material itself. In this work, we take CoCrSn as an example to study the stability of mechanical and half-metallic properties. This study is expected to provide a new perspective for the study of similar materials.

2. Computational Details

First-principles calculations are carried out using the full potential linearized augmented plane wave method (FP-LAPW) with the generalized gradient approximation as implemented in Vienna Ab-initio Simulation Package (WIEN2K). [8] The generalized gradient approximation (GGA) with Perdew–Burke–Ernzerhof as adapted for solids (PBE-sol) [9] is used to treat the electron exchange and correlation. The 12 atoms in the C_{1b} unit cell composed of four Co, four Cr, and four Sn atoms were considered for the self-consistency calculations. The valence electron configurations $3d^7 4s^2$ for Co, $3d^5 4s^1$ for Cr and $5s^2 5p^2$ for Sn were used in calculations. The total number of plane wave employed in the calculation was determined by taking the limit of $R_{MT} * K_{max} = 7.0$ (R_{MT} being the muffin-tin sphere radius and K_{max} is the maximum amplitude of lattice vector taken for plane wave). For all calculations, a k-space mesh of $10 \times 10 \times 10$ k-points were used in the irreducible Brillouin zone. The self-consistent cycle is considered converged when the total energy of the material is stable within 1.0×10^{-4} Ry.

we also consider the Hubbard U correction (GGA + U) in electronic structure calculations, where optimization of Hubbard U was carried out in such a way as to render the correct magnetic moment according to Slater-Pauling rule, accordingly the values of effective U parameter was determined as $U_{eff} = U - J$ where U indicates the Coulombic part and J the exchange part of the Hubbard U energy. The optimized values of U_{eff} were 0.1411 Ry and 0.1169 Ry for Co and Cr respectively. The selection of these values was based on the fact that they return values of total magnetic moments per unit cell which is consistent with the Slater-Pauling rule. We have run scf calculations with various values of effective U watching the total angular momentum per unit cell and the above value was selected accordingly. The effect of spin-orbit coupling was ignored in all our calculation since its effect has turned out to be so marginal, which is expected since neither rare earth nor heavy atoms were contained in the structures. We adopted GGA approximation according to Perdew Burk Ernzerhof parameterization adapted for solids (PBE-sol) [9]. since it has rendered results closer to previous studies.

3. Result and Discussion

3.1. Structural properties

In general, the half-Heusler compounds XYZ crystallize in the form of zinc-blende sub lattices where the octahedral sites are occupied, and crystallize in the face-centered

cubic $C1_b$ structure with the space group $F-43m$. In half-Heusler compound X, Y, and Z atoms occupy the lattice fractional $(1/4, 1/4, 1/4)$, $(0, 0, 0)$, and $(1/2, 1/2, 1/2)$ sites respectively and the $(3/4, 3/4, 3/4)$ site is empty [10] as shown in **Fig. (1)**

Table 1. The positions of Cr, Co and Sn atoms.

Atom	Wyckoff position	Site symmetry	Atomic coordinates		
			x	Y	z
Cr	4c	F-43m	0.25	0.25	0.25
Co	1a	F-43m	0.0	0.0	0.0
Sn	1b	F-43m	0.5	0.5	0.5

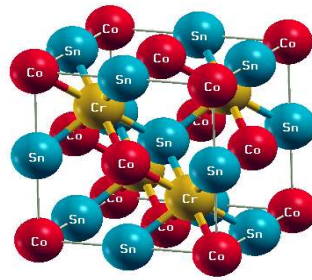


Fig. 1 The crystallographic structure of cubic CoCrSn

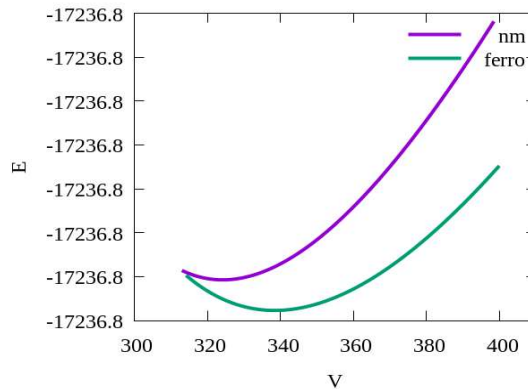


Fig. 2 Energy vs. unit cell volume of CoCrSn

Energy minimization versus unit cell volume was carried out for both the GGA and GGA+U approximations considering spin polarized (i.e. ferromagnetic) and non-spin polarized (non-magnetic) ground states. The energy versus volume curves hence calculated are illustrated in **Fig 2**. It can be seen from **Fig 2**, that the lowest energy curves correspond to the ferromagnetic

(FM) state for both cases, which means that the (FM) state is the more favorable ground state energetically. We can hence conclude that the ground state of half-Hausser compound CoCrSn is ferromagnetic.

The total energy versus volume data is fitted to the empirical Birch Murnaghan equation of state [11]

$$P(V) = \frac{3B_0}{2} \left[\left(\frac{V_0}{V} \right)^{\frac{7}{3}} - \left(\frac{V_0}{V} \right)^{\frac{5}{3}} \right] \left\{ 1 + \frac{3}{4} (B'_0 - 4) \left[\left(\frac{V_0}{V} \right)^{\frac{2}{3}} - 1 \right] \right\} \quad (1)$$

where P is the pressure, V_0 is the reference volume, V is the deformed volume, B_0 is the bulk modulus, and B'_0 is the derivative of the bulk modulus with respect to pressure. The bulk modulus and its derivative are usually obtained from fits to experimental data and are defined as

$$B_0 = -V \left(\frac{\partial P}{\partial V} \right)_{P=0} \quad \text{and} \quad B'_0 = \left(\frac{\partial B}{\partial P} \right)_{P=0}$$

from which the equilibrium lattice constants a_0 are obtained and listed in **Table 1**.

, however, the lattice constants of CoCrSn are very close to the previous theoretical investigations [13]. **Table. 3** displays the inter-atomic distances in the unit cells of alloy CoCrSn in energy minimized ground state.

Table 2. Optimized structural parameters of cubic CoCrSn

Parameter	PBEsol-GGA	PBEsol-GGA+U	Previous
a_0 (Å)	5.8540	5.8529	5.807 *
V_0 (Å ³)	338.9579	338.1651	-----
B_0 (GPa)	117.2789	115.9071	126.4*
B'_0 (GPa)	4.4098	4.6640	3.888*
E_0 (Ry)	-17236.8177	-17236.8175	-----

* Ref [10]

Table 3. Optimized bond distances in Å of cubic CoCrSn

Bond	GGA_sol (Å)	GGA_sol+U (Å)
d_{Co-Co}	5.859	6.1516
d_{Co-Cr}	2.5349	2.6637
d_{Co-Sn}	2.9270	3.0758
d_{Cr-Sn}	2.5349	2.6637

3.2. Electronic structure

To give an insight on the properties of compounds under investigation, the electronic energy band structures as well as the total, atomic and orbital densities of states were calculated in view of both GGA and GGA+U approximations. In the rest of this section sections, each case is presented and discussed separately.

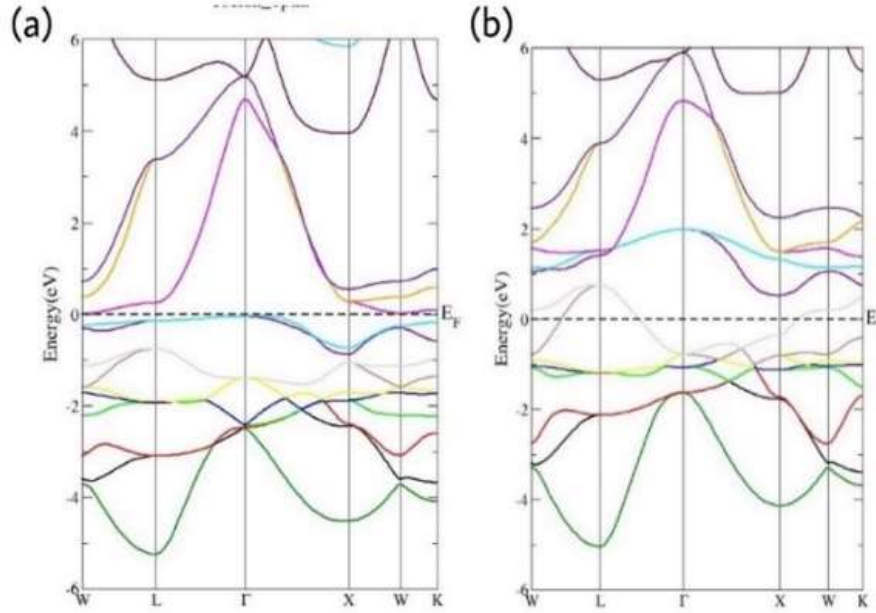


Fig. 3 Band structure for CoCrSn at equilibrium lattice constant for (a) spin up and (b) spin down panels

The GGA calculated band structure of spin polarized ground state of CoCrSn is shown in **Fig.3** where part (a) of the figure represents the spin majority and (b) the spin minority band structures, (in **Fig. 3** and henceforth, the Fermi level is set to zero). The figure reveals an almost flat band directly under the Fermi level at Γ which is 2 fold degenerate at W L Γ X high symmetry point of the first Brillouin zone, but not at K this band depicts a Γ_{12} symmetry character (F-43m) and is dominantly occupied by d_{eg} electron of Cr and Co atoms. A 2-fold degenerate band is also reported at 1.5 eV below the Fermi level at Γ point, the upper branch of which is seen to be 2-fold degenerate at L and X, Where the lower one is none-degenerate but highly overlapped by Co-d and Cr-d band that is a 2-fold degenerate at Γ , L and X. Above Fermi level there is a 3-fold degenerate band Γ_{15} ($d_{t_{2g}}$). It is obvious that the Fermi level crosses energy bands for both spin majority and minority bands hence showing a metallic character. A glance at **Fig. 4** should assert this finding.

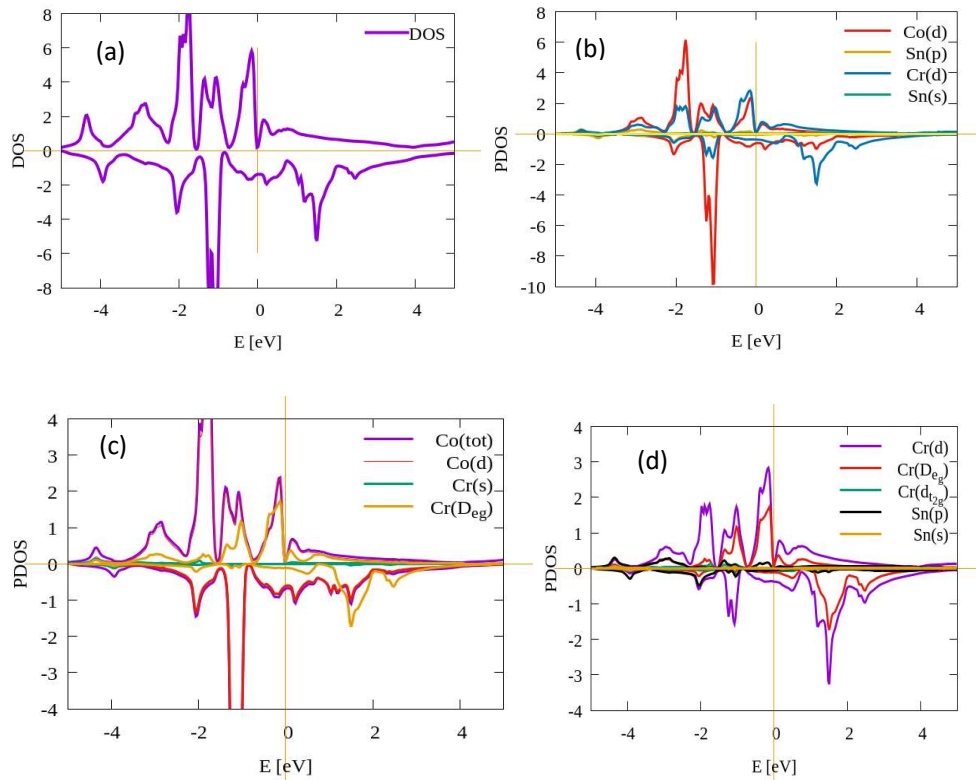


Fig. 4 Total and Partial Density of state of CoCrSn at equilibrium lattice constant.

To gain further insight on this picture we have represented total and multiple cases of the partial densities of states in **Fig. 4** where the Total and partial DOS plots show that the band occupying the region from -3.0 eV to 0.0 eV in both the majority and minority spin panels is dominantly occupied by 3d orbital of Co, which are strongly hybridized with Cr-3d and Sn-p, the Co-3d dominance is even stronger in the sub region from -1.5 eV to -0.5 eV with stronger d-d and p-d hybridization indicating an indirect (Cr-d)- (Co-d) exchange coupling through Sn-p orbital.

In contrast, the valence electrons attributed to the Cr site exhibit a pronounced localization at -1.5 eV (d_{eg}) in the spin-up panel. The occupation is close to zero at -1.0 eV in the majority and minority panel. It is to be noted that the Sn-p orbital moderately occupies the small region around -4.0 eV and the region from -3 to -1.5 eV. On the other hand, the partial DOS in the majority spin state show a remarkable dominance of the Cr-d (in particular the d_{eg} states) orbital in the occupied band from 0.0 eV to -1.0 eV with dismal hybridization with Co -d orbitals, while in the bands from -1.0 eV to -1.8 eV and -1.8 eV to 3.0 eV the Co-d dominates the occupation with strong of (Co-d) - (Cr-d) hybridization observed in both band. The unoccupied bands (of the majority spin) above Fermi level are dominated by Cr d states strongly hybridized with Co-d and in the range from 0.0 eV to 1.0 eV and steeply decreasing upon going to higher states. Meanwhile, in minority spin panel the unoccupied region from 0.0 eV to 4.0 eV exhibit a (Co-d) -(Cr-d) while the higher region around 1.5 eV and hybridization. We also see that the occupation of $Cr_{t_{2g}}$ is very weak. **Fig. 4** shows the spin polarized DOS for GGA based calculation the Figure show an important phenomenon that is the existence of a zero density of states at Fermi level in the majority spin but no marked band gap while in the minority the

behavior is completely metallic that is an indication that this alloy may tend to earn half metallic nature in some different circumstances or even with enhanced method of calculation. The electrons responsible for the metallic behavior just reported above are Cr-d electron as seen from the PDOS depicted by **Fig.4**.

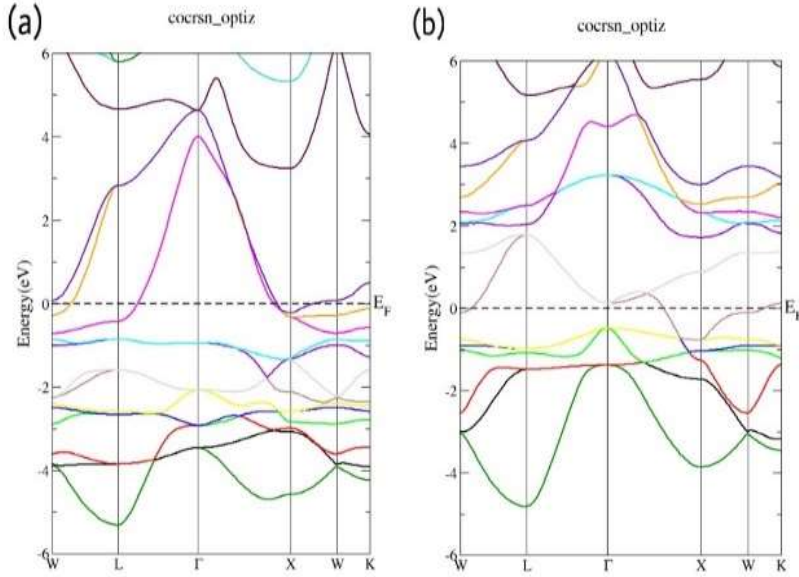


Fig 5. Band structure for CoCrSn at equilibrium lattice constant GGA+U for (a) spin up and (b) spin down

To make further insights on the effect of incorporating the Hubbard U correction on the electronic structure of the CoCrSn alloy, we have also represented the band structure of spin polarized ground state based on GGA+ U calculation in **Fig. 5** where part (a) of the figure represents the band structure for spin majority and (b) for the spin minority. In addition, the total, atomic and orbital densities of states for GGA+ U calculation are illustrated in **Fig. 6** (a)(b)(c)(d).

Fig. 5 (a) reveals an almost flat band under the fermi level (≈ 0.6 eV) at Γ point of the first Brillouin zone. It is also observed that the Γ_{12} band remains degenerate at Γ . The 2-fold degenerate Γ_{12} band is populated by d_{eg} – electron state of the Cr atoms while Γ_{15} is mainly occupied by a meagre population by d_{t2g} states of Cr atoms. The Γ_{12} which already crosses the Fermi level with GGA calculation is now shifted up by around 0.5 eV when using GGA+ U approach to further cross Fermi level yielding obvious metallic character. It is also noted that the structure in the energy range from ~ -2.0 eV to ~ 2.0 eV (which is the range mainly populated by d- electron states) exhibits an upward shift as whole by ~ 0.8 eV after the incorporation of U -correction. The Γ_{12} band that shifted up which reveals a 3d character, remains crossing the Fermi level and its degeneracy at Γ and L seemed unaffected.

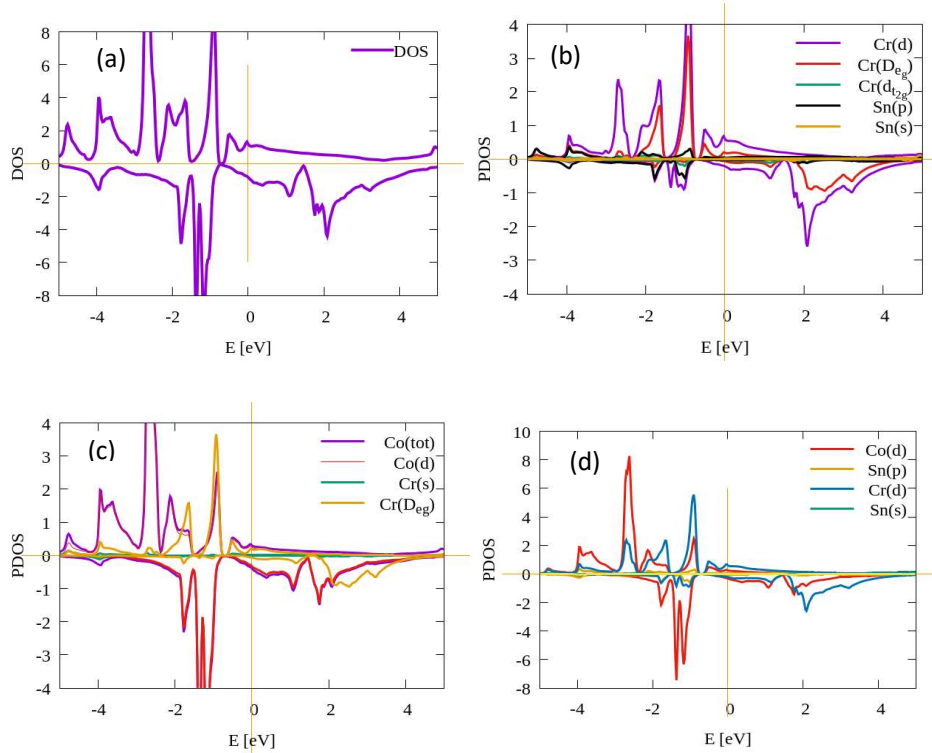


Fig 6. Total and partial Density of state of CoCrSn at equilibrium lattice constant GGA+U.

To further elucidate the picture, total as well as many atomic and orbital densities of states are represented in **Fig. 6** where the Total and partial DOS plots show that the band covering the region from -5.0 eV to 5.0 eV for spin-down states is occupied by $3d_{eg}$ orbital of Co and dominated by Co-d while the energy range from -3.0 eV to 0.0 eV in the spin down is highly occupied by Co-3d orbitals with strong hybridization with Cr-3d and Sn-p. The Co-3d dominance is further remarked in the sub region from -2.0 eV to -1.0 eV with a slight d-d and p-d hybridization which implies a relatively moderate Cr-d Co-d indirect exchange coupling mediated by Sn-p electrons. We attribute the decline in hybridization to the shift occurring on d- electrons due to the application of Coulomb part of U correction. On the other hand, the valence electrons attributed to the Cr site exhibit a pronounced localization at -1.0 eV (d_{eg}) in the spin-up panel. The occupation is close to zero at -0.8 eV in the majority and minority panel. It is to be noted that the Sn-p orbital moderately occupies the small region around -4.0 eV and the region from -3.0 eV to -1.5 eV and the small region around -1.0 eV. On the other hand, the partial DOS in the majority spin state show a remarkable dominance of the Cr-d (in particular the d_{eg} states) orbital in the occupied band at -1 eV with obvious hybridization with Co $-d$ orbitals, while in the bands from -1.5 eV to -2.0 eV and -2.0 eV to 4.0 eV the Co-d dominates the occupation. It is to be noted that the Sn-p orbital occupies the region from -3.0 eV to -1.0 eV and the region from -5.0 eV to -3.5 eV. The unoccupied bands (of the majority spin) above Fermi level are dominated by Cr-d states strongly hybridized with Co-d and in the range from 0.0 eV to 2.0 eV and the occupation decreases in higher states. Meanwhile, in minority spin panel the occupied region from 0.0 eV to 4.0 eV exhibit a (Co-d)-(Cr-d) character while in the higher region around 2.0 eV. We also see that the occupation of Cr_{t2g} is very weak. The change in partial densities of states due to the Hubbard U can in short be attributed to the fact that the exchange correlation interaction with as corrected by effective U parameter might have excreted a downward energy shift for sin-up and upward for the spin-down states.

Spatial distribution of charge density in the unit cell was examined by taking its two dimensional projections in (100) and (110) planes as depicted in **Fig. 7** and **Fig.8** respectively. Isolated density contours around each atom indicate Sn-Cr and Sn-Co ionic bonding we have proposed this bonding scheme according to the fact that Sn has the highest electronegativity 1.96 among the three constituents confirming our statement of the metallic nature of the system.

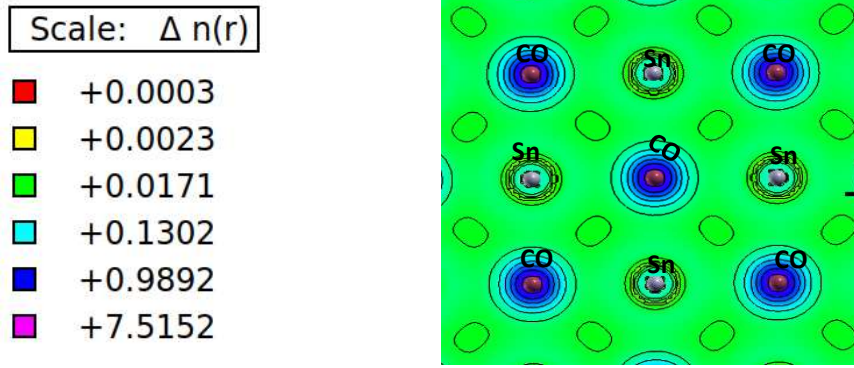


Fig. 7. Spatial change density distribution in (100) plane of the unit cell

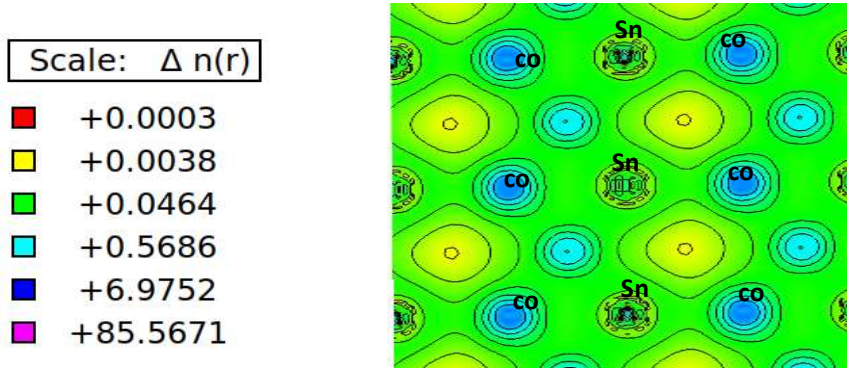


Fig. 8. Spatial charge density distribution in (100) plane of the unit cell.

3.3. optical properties

The optical properties of CoCrSn compound, such as the dielectric function, electron loss function (ELOSS), reflectivity and absorption coefficient were determined using generalized gradient approximation (GGA) and GGA+U [14,15]. The essential quantity to calculated here is the imaginary part of the dielectric function ($\text{Im } \epsilon$). If all intra-band transitions contribution is considered, then:

$$\text{Im}\epsilon_{ij}^{\text{[inter]}}(\omega) = \frac{\hbar^2 e^2}{\pi m_e^2 \omega^2} \sum_n \int dk \langle \Psi_k^{c_n} | p^i | \Psi_k^{v_n} \rangle \langle \Psi_k^{v_n} | p^j | \Psi_k^{c_n} \rangle \sigma(E_k^{c_n} - E_k^{v_n} - \omega) \quad (2)$$

The expression (2) above includes the summation of inter-band transitions from occupied valence levels with eigen-state $|\Psi_k^{v_n}\rangle$ and eigen-value $E_k^{v_n}$ to unoccupied conduction levels with eigen-state $|\Psi_k^{c_n}\rangle$ and eigen-value $E_k^{c_n}$ (where p stands for momentum operator), as well as

intra- band transition. The other quantities such as the refraction, absorption and reflection indices can be obtained from the real and /or imaginary parts of the dielectric function. From the imaginary part of dielectric tensor, one can determine the corresponding real part via the Kramer's–Kronig relations

$$\text{Re } \varepsilon_{ij}^{[\text{inter}]}(\omega) = \sigma_{ij} \frac{2}{\pi} \text{P} \int_0^\infty \frac{\omega' \text{Im } \varepsilon_{ij}(\omega)}{\omega^2 - \omega'^2} d\omega' \quad (3)$$

where, P indicates the principal value of integral. On the other hand, the contribution of metallic intra-band transitions is described by the relation:

$$\text{Im } \varepsilon_{ij}^{[\text{intra}]}(\omega) = \frac{\Gamma \omega_{\text{plij}}^2}{\omega(\omega^2 + \Gamma^2)}, \text{Re } \varepsilon_{ij}^{[\text{intra}]}(\omega) = \frac{\omega_{\text{plij}}^2}{\omega(\omega^2 + \Gamma^2)} \omega_{\text{pl}}^2 \quad (4)$$

In equation (4), Γ represents the lifetime broadening in Drude model, ω_{pl} denotes plasma frequency. The total dielectric function including all interband and intraband transitions is obtained as follows:

$$\varepsilon(\omega) = \varepsilon_{ij}^{[\text{inter}]}(\omega) + \varepsilon_{ij}^{[\text{intra}]}(\omega) \quad (5)$$

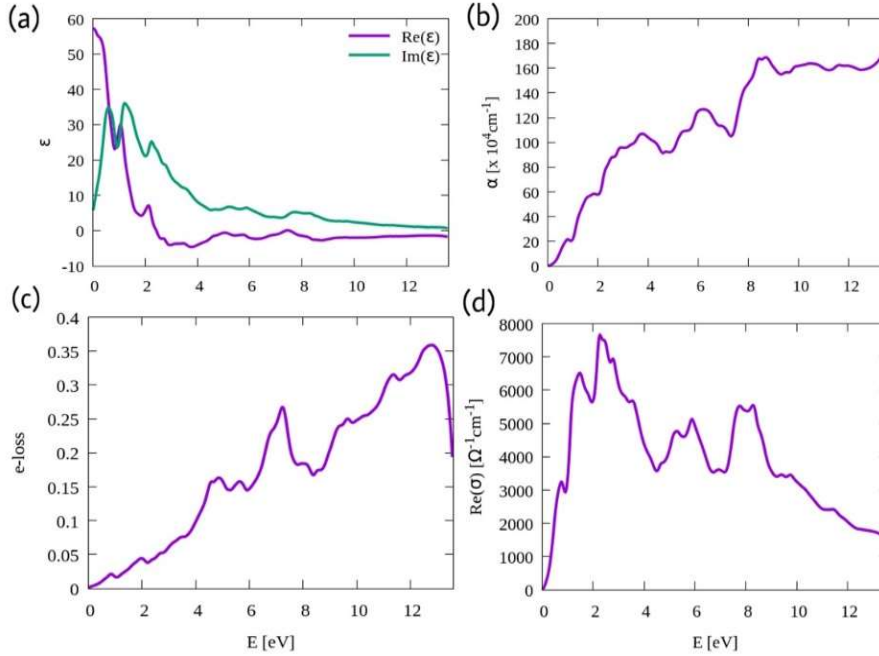


Fig 9. (a)The dielectric permittivity (b) absorption (c) energy loss electron (d) conductivity for CoCrSn (GGA).

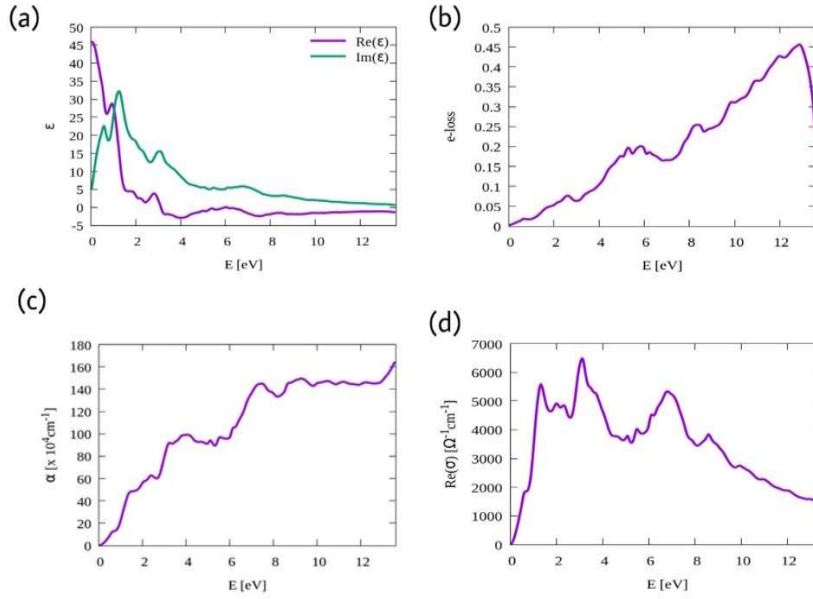


Fig10. (a)The permittivity (b) absorption (c) energy loss electron (d) conductivity for CoCrSn (GGA+U).

The GGA results of optical properties, namely: the dielectric permittivity, optical absorption, electron energy loss and optical conductivity are presented in **Fig. 9** (a), (b), (c) and (d) respectively, while the corresponding GGA+U results are presented in **Fig. 10** (a), (b), (c) and (d) in the same respective order. From **Fig. 9** (a) and **Fig. 10** (a), it can be seen that the static part of dielectric function tends to extremely high values for GGA based calculation; implying that this alloy has manifested almost metallic behavior in this energy range and that the negative value of $\text{Re } \epsilon(\omega)$ in the energy range after 2.5 eV (GGA) and 3.0 eV (GGA+U) reveals the loss of light transition for this alloy. we see in **Fig. 9** (a) and **Fig. 10** (a), that $\text{Re } \epsilon(\omega)$ returns roots in the 2.5, 5.0 eV and 7.0 eV energy values for GGA approximation while in GGA+U calculations $\text{Re } \epsilon(\omega)$ roots correspond to 3.0 eV and 6.0 eV photon energies. The occurrence of $\text{Re } \epsilon(\omega) = 0$ roots has an important significance as far as the medium response to light is concerned, which is that the compound does not respond to incident light for these root values due to the Plasmon oscillations. Comparing **Fig. 9** (a) and **Fig. 10** (a), with peaks of electron energy loss curves **Fig. 9** (c) and **Fig. 10** (c), respectively, we can conclude that plasmon oscillation occurs in 2.0, 5.0 eV and 7.0 eV for GGA calculation, while, in GGA+U results, plasmon oscillation takes place at in 3.0 eV and 6.0 eV. A common feature for both GGA and GGA+U calculations is that the main positive response occurs in infrared range (up to 1.6 eV) and in the visible (1.6 eV–3.1 eV) spectrum frontiers for CoCrSn. But, for values of energy greater than 3.1 eV, the $\text{Re } \epsilon(\omega)$ is negative for CoCrSn. Thus the compound would be opaque for this rang of ultra violet frequency $\sim 7.5 \cdot 10^{14}$ Hz. The sharp peak in electron energy loss right after ~ 8.0 eV is the evidence of opaqueness of the compound for the corresponding range of frequency. As incident photon energy increases to UV domain (~ 4.8 eV), there are other peaks for this compound. But, by further stimulation, the amplitude of peaks decreases and practically does not lead to electron transition in this energy range. By a glance at **Fig. 9** and **Fig. 10** we can see that the permittivity, absorption, electron energy loss and conductivity curves of CoCrSn begin from very low incident photon energies for both GGA and GGA+U calculations. This behavior is expected, due to metallic characteristic anticipated for CoCrSn.

In the infrared and visible limits, the absorption and electron energy loss increase in a natural manner, as for conductivity we see a strong increase. In ultra violet UV limit absorption continues to increase and the electron energy loss makes a peak at ~ 7.0 eV and decreases sharply after ~ 12.0 eV, as for conductivity, a sharp decrease begins from 3.0 eV to 5.0 eV and there are two peaks at 6.0 eV and 8.0 eV and then the conductivity decrease continues naturally. Also from **Fig. 9** (a) and **Fig. 10** (a), it is obvious that the imaginary part of permittivity makes an increase in infrared limit with two peaks in visible limit and then begins to decrease, while the real permittivity starts very large and decreases sharply and at 2.5 eV in GGA while at 3.0 eV it stabilizes when GGA + U approximation being utilized. and the imaginary permittivity tend to be stable at 4.0 eV in GGA and after 4.5 eV in GGA+U. An overlap between imaginary and real parts of permittivity is observed in GGA results with a slight shift upon implementing GGA+U.

Conclusion

In the present work, we have investigated the structural, electronic and optical properties of the new half-Heusler alloy CoCrSn using first-principle calculations based on the FP-LAPW method. Two approximations were used to treat the exchange correlation potential: GGA and GGA+U approximations. The equilibrium lattice parameters, bulk modulus, its first pressure derivative and minimum total energy are evaluated in ferromagnetic (FM) and nonmagnetic (NM) states. The structural analysis revealed that the ferromagnetic is the most stable ground state of the studied material. The results of the electronic properties unveil a half-metallic behavior using GGA and GGA+U, respectively. The optical properties, the real and imaginary parts of dielectric function, electron energy loss, absorption coefficient and optical conductivity are calculated whereas, all the interband and intraband transitions are considered. The peaks in the imaginary part of dielectric are essentially resulting from interband transitions. Curves of the real part of dielectric function versus energy show that there is metallic property in very low energies; Moreover, the amount of light absorption increases due to the low electron transition rate.

ACKNOWLEDGMENT

Researcher would like to thank Deanship of Scientific Research and the Deanship of Graduate Studies at Qassim University for motivating the publication of this paper.

Reference

- [1]. P. J. Webster and K. R. A. Ziebeck, *Alloys and Compounds of d-Elements with Main Group Elements* (Springer, Berlin, 1988), p. 75.
- [2]. K. R. A. Ziebeck and K. U. Neumann, *Magnetic Properties of Metals* (Springer, Berlin, 2001), p. 64.
- [3]. E. S, a, so ̇glu, L. M. Sandratskii and P. Bruno, *J. Appl. Phys.* 98 (2005) 063523.
- [4]. M. Zhang, X. Dai, H. Hu, G. Liu, Y. Cui, Z. Liu, J. Chen, J. Wang and G. Wu, *J. Phys.: Condens. Matter* 15 (2003) 7891.
- [5]. I. Galanakis, E. Sasioglu and K. Oezdogan, *Phys. Rev. B* 77 (2008) 214417.
- [6]. Z. Y. Yao, Y. S. Zhang and K. L. Yao, *Appl. Phys. Lett.* 101 (2012) 062402.
- [7]. L. Feng, E. K. Liu, W. X. Zhang, W. H. Wang and G. H. Wu, *J. Magn. Magn. Mater.* 351 (2014) 92.
- [8] K. Schwarz, P. Blaha, G.K.H. Madsen. *Electronic structure calculations of solids using the WIEN2k package for material sciences. Computer Physics Communications* 147 (2002) 71–76
- [9] Lv S H, Li H P, Liu X J, Han D M, Wu Z J and Meng J 2010 *J. Phys. Chem. C* 114 16710
- [10] Hai-Ming Huang, Ze-Dong He, Chuan-Kun Zhang and Shi-Jun Luo, *Mechanical and half-metallic properties of half-Heusler CoCrSn*, *Modern Physics Letters B*, 32, 1, 1850006 (2018)

- [11] Hai-Ming Huang, Chuan-Kun Zhang, Ze-Dong He, Jun Zhang, Jun-Tao Yang, and Shi-Jun Luo, Electronic and mechanical properties of half-metallic half-Heusler compounds CoCrZ ($Z = \text{S, Se, and Te}$), Chinese Physics B, 27,1, 017103, (2018).
- [12] Murnaghan F D 1944 Natl. Acad. Sci. 30 244
- [13] Li Y, Yuan H K, Xia J, Zhong M, Kuang A L, Wang G Z, Zheng X R and Chen H 2015 Eur. Phys. J. Appl. Phys. 70 31001
- [14] Fox M. Optical Properties of Solids. New York: Oxford University Press; 2001.
- [15] Wooten F. Optical Properties of Solids. New York: Academic Press; 1972